Lab on a Chip

RSC Publishing

PAPER

View Article Online
View Journal

# Low-voltage manipulation of an aqueous droplet in a microchannel *via* tunable wetting on PPy(DBS)

Cite this: DOI: 10.1039/c2lc40621g

Yao-Tsan Tsai, Chang-Hwan Choi and Eui-Hyeok Yang*

Received 30th May 2012,
Accepted 22nd October 2012

DOI: 10.1039/c2lc40621g

www.rsc.org/loc

This paper presents experimental results and analyses on the controlled manipulation of a liquid droplet. The droplet was manipulated upon local reduction and oxidation (redox) of dodecylbenzenesulfonate doped polypyrrole (PPy(DBS)) in an immiscible organic fluid of bulk dichloromethane (DCM, $CH_2Cl_2$). The electrochemically tunable wetting property of PPy(DBS) permitted liquid droplet manipulation at very low voltages (−1.5 V to 0.6 V). In particular, the actuation behavior of a salt water droplet upon redox of PPy(DBS) in a microchannel configuration was characterized and analyzed. The controlled lateral transport of the droplet was successfully demonstrated in a slightly tilted microchannel configuration.



## 1. Introduction

Fluid transportation is the most basic operation within microfluidic devices.[1] Several techniques have been shown to manipulate fluids, such as capillary driven test strips, microfluidic valves, pressure driven channels, electro-osmosis, dielectrophoresis (DEP), and electrowetting on dielectric (EWOD).[2–4] In contrast to continuous-flow systems, droplet-based microfluidics such as EWOD have been used to manipulate individual droplets.[5] On the microscale, capillary forces dominate liquid behavior; hence the control of interfacial energies becomes important for manipulating droplets in microfluidic systems. EWOD techniques have been shown to manipulate microliter-sized individual droplets on dielectric surfaces by electrostatic modulation using arrays of electrodes.[6] Without increasing device size or complexity, various fluidic functions and reactions were successfully demonstrated with EWOD devices including transportation, mixing and separation.[7–9] However, they typically require relatively high actuation voltages (12–80 V),[7–11] which potentially hamper their compatibility with biofluids and biomedical applications as well as their portability for direct field operation (*e.g.*, using a standard sized battery).

In order to realize low voltage manipulation of microfluidic droplets, conjugated polymers have been considered one of the most promising routes.[12–14] Conjugated polymers can change their mechanical and electrical properties when electrochemically "doped" (*i.e.*, undergoing a reduction and oxidization process).[15–20] An earlier report using polyaniline shows the control of the contact angle of a water droplet.[12] However, the surface states before and after the reduction and oxidation are both hydrophilic. Thus, the minute contact angle change would not result in the creation of sufficient force for droplet manipulation. In contrast, dodecylbenzenesulfonate (DBS) doped polypyrrole (PPy), (PPy(DBS)), exhibits a large difference in surface energy under reduction or oxidation, whereby the surface state can be switched entirely from hydrophilic to hydrophobic due to the re-orientation of the surfactant dopant molecules, $DBS^-$.[16–19] Recently, we have demonstrated *in situ* manipulation of a liquid droplet using electrochemical redox of PPy(DBS) at ultra-low voltages (<1 V).[21] Although it was successfully shown that the electrochemical redox process on PPy(DBS) results in efficient manipulation of a liquid droplet, the tested liquid droplet was an organic fluid (dichloromethane, DCM). Since biofluids such as blood, sweat, tears and serum are water-based,[22] there is a strong need for research on the manipulation of aqueous droplets for the implementation of such microfluidic applications.[6,23,24] Moreover, such biofluids contain salt ions. The manipulation of biofluids using PPy(DBS) redox would be ideal for such a liquid composition, since reduction and oxidation reactions of PPy(DBS) are enabled by the induction of sodium ions.[22] Also, low voltage stimuli are essential in such diagnostic applications.[25,26] In this paper, we investigate the actuation mechanism of an aqueous droplet on PPy(DBS) undergoing reduction and oxidation reactions, and demonstrate the lateral transport of a salt water droplet in a microchannel configuration.

## 2. Device fabrication and experimental setup

To study the actuation behavior of a droplet of salt water in the redox process of PPy(DBS), a microchannel configuration was constructed within an organic fluid, bulk dichloromethane

*Department of Mechanical Engineering, Stevens Institute of Technology, Hoboken, NJ, 07030, USA. E-mail: Eui-Hyeok.Yang@stevens.edu; Fax: +1-201-216-8315; Tel: +1-201-216-5574*

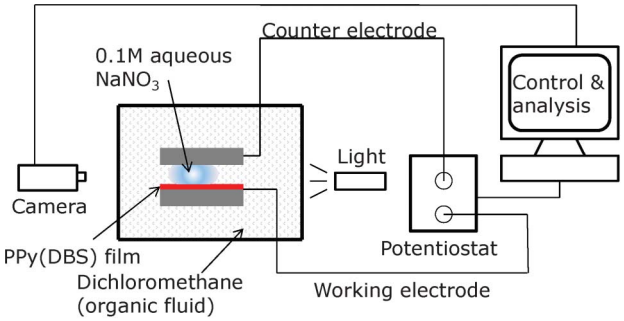


**Fig. 1** Schematic configuration of the experimental setup for droplet manipulation. The microchannel assembly consisting of parallel plates was set in an electrode system within a DCM environment.

(DCM, $CH_2Cl_2$), which is a widely used water-immiscible organic solvent for liquid–liquid extraction applications (Fig. 1). Since dichloromethane is biocompatible, a water–dichloromethane emulsion has been used for drug delivery.[27] In this liquid–liquid system, DCM acts as a filler fluid, preventing droplet evaporation and reducing surface contamination.[28] The bottom plate, a PPy(DBS) electrode, was fabricated *via* electropolymerization from the aqueous monomer pyrrole. The detailed synthesis of the PPy(DBS) electrode is described elsewhere.[21] A brief summary is as follows: first, Au/Cr metallization (30 nm and 10 nm in thickness, respectively) was performed on a silicon/silicon dioxide (90 nm) substrate *via* electron beam evaporation (PVD 75, Kurt J Lesker). The diced substrate was then submerged in a freshly prepared aqueous pyrrole solution (0.1 M pyrrole and 0.1 M sodium dodecylbenzenesulfonate). A 263A potentiostat (Princeton Applied Research, Oak Ridge, TN) was used to potentiostatically deposit PPy(DBS) at 0.47 V to obtain a 200 nm-thick uniform PPy(DBS) layer . The thickness of the PPy(DBS) film was precisely controlled by adjusting the amount of applied charge ($\sim$0.05 C cm$^{-2}$). After polymerization, the PPy(DBS) coated substrate was then rinsed with deionized (DI) water and dried with nitrogen gas.

Another Au coated silicon/silicon dioxide chip was used as the top plate (Fig. 2a). 3M Scotch brand tape was used as a non-conductive spacer, placed between the two plates to construct a microchannel with the vertical gap of 500 μm (Fig. 2b). To manipulate an aqueous droplet, the PPy(DBS) substrate was set as a working electrode and the top Au electrode as a counter electrode. The 263A potentiostat was programmed with pulse potentials controlled by PowerSuite software (Princeton Applied Research). A 0.1 M $NaNO_3$ aqueous droplet (2–3 μL) was dispensed between the two plates using a microsyringe with a fine needle (Standard type 304 stainless steel needle, Ramé-hart). For this study, a $NaNO_3$ electrolyte was adopted, since sodium ions possess higher mobility than other ions, such as $TBA^+$ or $K^+$ ions.[13] The assembled microchannel setup was then immersed in a DCM environment (Fig. 2c). The redox reactions of PPy(DBS) typically occur in a voltage range of $\pm$1 V.[21] In this study, the working electrode potential was adjusted between −1.5 V and +0.6 V with the frequency varied within 0.2–4 Hz. Droplet manipulation experiments were performed in two configurations. We first considered droplet behavior on a leveled (non-tilted) stage. Then we investigated a tilted stage in order to create an 'unbalanced' condition for transporting a droplet.

## 3. Results and discussion

### 3.1 Manipulation of a water droplet in a leveled microchannel configuration

Initially (when no voltage was applied), the aqueous liquid droplet exhibited a symmetric disk-like droplet shape as shown in Fig. 3a. When a reductive potential (−1.5 V) was applied, the contact angle of the droplet increased by $\sim$2° immediately (<1 s), and the contact diameter decreased by about 5% (Fig. 3b). When the reductive potential was applied over 10 s, the droplet contact line was pinned on the PPy(DBS) electrode and led to a decrease in the droplet contact angle by $\sim$13° (Fig. 3c). In particular, the droplet was deformed to a "funnel" shape with prolonged application of the reductive potential (Fig. 3d–f). When the reductive potential was removed or an oxidation voltage was further applied, the droplet immediately (<1 s) reverted to its original state (Fig. 3g). These results suggest that there are two distinct wetting dynamics involved in the droplet behaviors, *i.e.*, the initial stage where the droplet shrinks with a slight increase of

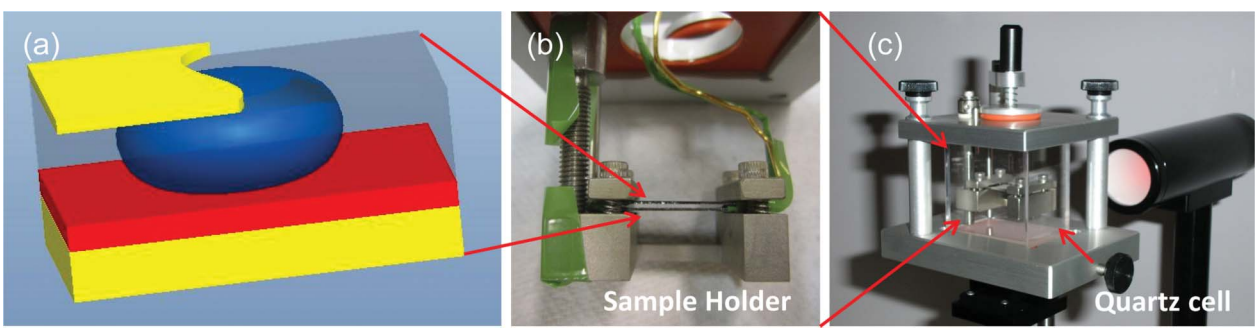


**Fig. 2** (a) Schematic of microchannel configuration. (b) Sample holder containing the microchannel assembly. (c) Assembled microchannel setup immersed in a quartz cell pre-filled with DCM with a goniometer (model 500, Ramé-hart, Netcong, NJ).

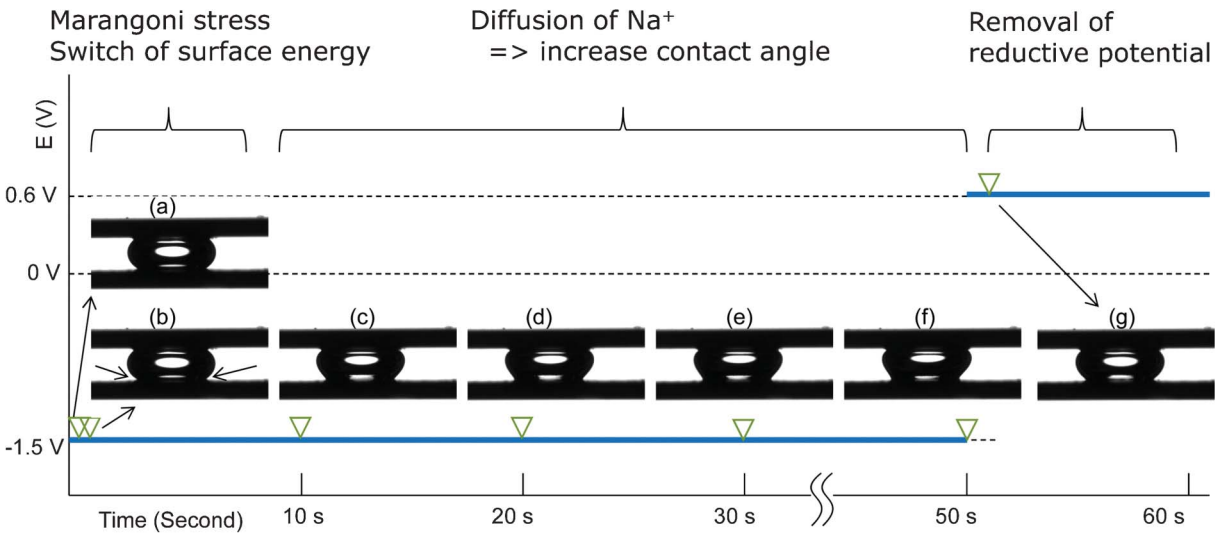


**Fig. 3** Captured images of an aqueous droplet in a microchannel within a DCM environment upon the continuous application of a reductive potential ($E = -1.5$ V). (a) Initially, an aqueous droplet resting with a symmetric shape in the microchannel. (b) The droplet receded with a slight increase in contact angle when a reductive potential was applied. (c–f) The droplet was further deformed to an asymmetric ''funnel'' shape. (g) The droplet reverted to its original state when an oxidative potential ($E = 0.6$ V) was applied.

contact angle (Fig. 3a–b), followed by the second stage where the asymmetric funnel-like droplet shape was developed with a slight decrease in contact angle (Fig. 3c–f). Our analysis suggests that the first stage is driven by the Marangoni stress created at the droplet contact boundary,[21] while the second stage is associated with the transient diffusion of sodium ions ($Na^+$) into the PPy(DBS) electrode layer.[21] A detailed analysis of the mechanisms of droplet deformation is in the following sections.

**3.1.1** Initial deformation in short reduction period. Before the reduction voltage was applied, the PPy(DBS) surface was in an oxidized state due to its low oxidation potential[29] (Fig. 4a). On the oxidized PPy(DBS) surface, the surfactant dopant molecules ($DBS^-$) are coupled to PPy chains *via* ionic bonding with polar (hydrophilic) sulfonic acid groups, allowing the non-polar (hydrophobic) dodecyl chains to thrust out from the polymer chains.[30,31] Oxidized PPy(DBS) possesses lower surface energy than reduced PPy(DBS) and this leads a water droplet to have a relatively large contact angle on the oxidized PPy(DBS) surface.[32,33] The surface state of PPy(DBS) can then be reversed *via* re-orientation of the DBS molecules *via* reduction.[34] Charge transport during the PPy(DBS) redox process is dominated by cations ($Na^+$), since $DBS^-$ anions are relatively immobile.[13,35] For complete reduction of a PPy(DBS) film, sodium ions ($Na^+$) in the liquid need to be transported into the PPy(DBS) for charge neutralization,[29] as represented in eqn (1).

$$\mathrm{PPy(DBS)} + \mathrm{Na^+} + \mathrm{e^-} \underset{\text{Oxidization}}{\overset{\text{Reduction}}{\rightleftharpoons}} \mathrm{PPy(DBS)^-Na^+} \quad (1)$$

When a salt water droplet is dispensed onto the PPy(DBS) surface, sodium ions would be available only on the area covered by the salt water droplet. Therefore, the PPy(DBS) surface underneath the droplet is fed by sodium ions from the salt water when the reductive potential is applied. In contrast, the PPy(DBS) surface exposed to DCM remains oxidized, since no sodium ions are available on the area outside the salt water droplet. This selective supply or blocking of sodium ions creates dissimilar surface states (or localized reduction) across the droplet contact boundary as shown in Fig. 4b. The surface tension gradient, *i.e.* the Marangoni stress across the contract boundary, causes the liquid to flow away from the region of low surface tension towards the region of high surface tension. Oxidized PPy(DBS) possesses lower surface energy than reduced PPy(DBS). Therefore, the induced Marangoni stress drives the contact boundary to retract inwards (*i.e.*, from the oxidized PPy(DBS) to the reduced PPy(DBS) surface). Then, the contact angle of the droplet increases from $\theta_{wo}$ to $\theta_{wo}'$ due to mass conservation (*i.e.*, to maintain the same volume of the droplet). Meanwhile, it is observed that the contact diameter at the top Au electrode side shows no significant change.

The initial droplet deformation behavior with the increase of contact angle can be explained by using a force balance equation at the contact point. Eqn (2) represents the force balance of the interfacial tensions at the three-phase contact point.

$$\gamma_{ws} + \gamma_{ow}\cos\theta_{wo} = \gamma_{os} \quad (2)$$

where $\gamma_{ws}$ is the interfacial tension between salt water and PPy(DBS), $\gamma_{ow}$ is the interfacial tension between DCM and salt water, $\gamma_{os}$ is the interfacial tension between DCM and PPy(DBS), and $\theta_{wo}$ is the contact angle of aqueous drop within DCM. When a reductive potential is applied to the working

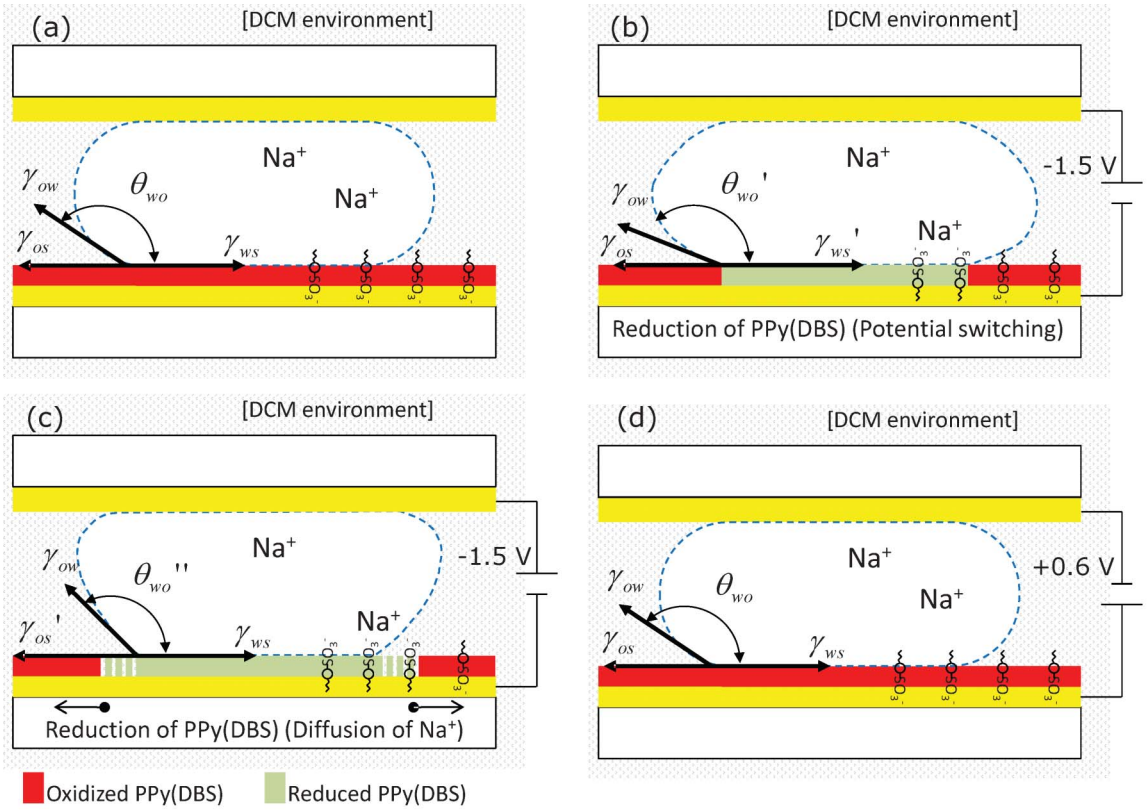


**Fig. 4** Conceptual schematic of droplet deformation under redox process. (a) An aqueous droplet is placed in a microchannel within a DCM environment. (b) When a reductive potential is applied, the contact boundary moves inwards due to Marangoni stress induced by the surface tension gradient across the droplet boundary. The droplet contact angle is then increased as the contact diameter is decreased. (c) The contact angle decreases when a reductive potential is applied for a prolonged time period (*e.g.*, more than 10 s), where the sodium ions gradually diffuse out through the PPy(DBS) layer and the reduction is propagated laterally. (d) The droplet reverts to the initial symmetric morphology once the PPy(DBS) layer is oxidized.

electrode and the PPy(DBS) surface underneath the droplet is reduced, the force balance at the new interface can be represented by eqn(3).

$$\gamma_{ws}' + \gamma_{ow}\cos\theta_{wo}' = \gamma_{os} \quad (3)$$

where $\gamma_{ws}'$ is the modified interfacial tension between salt water and reduced PPy(DBS) and $\theta_{wo}'$ is the new contact angle of aqueous droplet on the localized reduced PPy(DBS). Since reduced PPy(DBS) has higher surface tension (increased $\gamma_{ws}'$), the contact angle of the aqueous droplet ($\theta_{wo}'$) increases because $\gamma_{ow}$ and $\gamma_{os}$ remain unchanged.

**3.1.2** Funnel deformation in prolonged reduction period. With prolonged application of a reductive potential, sodium ions are expected to diffuse through the PPy(DBS) layer, not only vertically but also laterally. This lateral diffusion of sodium ions gradually reduces the nearby region of the PPy(DBS) surface, outside the initial contact boundary of the droplet (Fig. 4c). In previous reports by Wang and Smela,[18,19] such ion transportation parallel to the film surface has been already demonstrated during the redox reactions. The reported velocity of the propagation of the reduction was in the order of 1 μm $s^{-1}$.[18,19] Then, the surface tension gradient and the Marangoni stress across the droplet boundary are reduced and the new force balance can be described by eqn 4.

$$\gamma_{ws}' + \gamma_{ow}\cos\theta_{wo}'' = \gamma_{os}' \quad (4)$$

where $\gamma_{os}'$ is the interfacial tension between DCM and reduced PPy(DBS) and $\theta_{wo}''$ is the contact angle of the aqueous droplet immersed within DCM when the reductive potential is applied for a prolonged time. Since the reduced PPy(DBS) possesses higher surface energy,[21] the interfacial tension between DCM and reduced PPy(DBS), $\gamma_{os}'$, would increase. It would in turn decrease the contact angle of the aqueous drop in DCM, $\theta_{wo}''$, after sodium ions laterally diffuse into PPy(DBS) for the prolonged time (Fig. 4c). While the droplet contact angle decreases, the droplet shows no significant expansion (*i.e.*, an increase of contact diameter). Here, strong pinning effects on the reduced PPy(DBS) surface account for such a behavior, where the high surface energy[21] in the reduced PPy(DBS) holds the meniscus in place and facilitate the contact line pinning. In the meantime, the droplet contacting the top electrode maintains the same contact angle throughout the reduction, since no electrochemical reaction takes place at the interface of the Au electrode and the droplet.[21] Therefore, the strongly

 

pinned droplet with the lower contact angle would be pushed up and form the funnel-like geometry (Fig. 4c). When the reduction voltage is released or oxidation voltage is further applied, the droplet immediately (<1 s) reverts to the initial symmetric morphology since the surface tension gradient and the Marangoni stress at the droplet contact boundary has disappeared (Fig. 4d). The reverting process is faster than the prolonged reduction process, since the diffusion rate of ions in oxidized PPy(DBS) is different from that of reduced PPy(DBS). The details of PPy(DBS) redox were discussed by Wang and Smela,[18,19] such that oxidation of PPy(DBS) occurs faster than reduction of PPy(DBS).

### 3.2 Manipulation of a water droplet in a tilted microchannel configuration

While the funnel-like asymmetric deformation of an aqueous droplet along the vertical direction was demonstrated in a leveled microchannel *via* the low-voltage redox process of PPy(DBS), we also studied the manipulation of the aqueous droplet in a tilted microchannel configuration, in order to examine how the unidirectional buoyant force along the tilted direction would affect the droplet deformation and dynamics (Fig. 5). When the microchannel is tilted, a buoyant force is exerted on the aqueous droplet due to the difference in density compared to DCM and causes the droplet to move up along the tilted direction. This happens only if the tilting angle is greater than a critical angle that overcomes the static friction on the surfaces. If the angle is less than the critical angle, the droplet only deforms with a change of meniscus shape. For example, on the uphill side of the droplet, the contact angle of the aqueous droplet increases. However, if the contact angle is less than an advancing contact angle, the droplet meniscus remains pinned on the surface. On the downhill side, the contact angle decreases with the tilting. However, if the contact angle is still greater than a receding contact angle, the droplet on the downhill side also remains pinned on the surface. In order for a droplet to move up on a tilted surface, the buoyant force should be greater than the static friction force to 'depin' the droplet from the surfaces, and the droplet must both advance (on the uphill side) and recede (on the downhill side). The static friction force is proportional to contact angle hysteresis,[36,37] which is the difference between advancing and receding contact angles. Before we apply the reductive potential to the PPy(DBS) surface, we measured the critical tilting angle. Here, the critical tilting angle is the angle that induces transportation of the droplet solely due to the unidirectional buoyant force. We also measured the advancing and receding contact angles at the moment. For the aqueous droplet in the microchannel immersed in the DCM environment, the measured critical tiling angle was 25° with the advancing and receding angles being ~157° and ~133°, respectively. The corresponding buoyant force along the tilted direction for this natural movement is 3.4 μN for a 2.5 μL water droplet.

**3.2.1** Water droplet manipulation under constant potential. We first investigated the behavior of a water droplet under a constant reductive potential (−1.5 V) continuously applied to the PPy(DBS) electrode. Fig. 5 shows the experimental results measured at the tilting angle of ~7°, along with the schematics of the droplet behaviors. The tilting angle of 7° was the minimum angle to move the droplet during the experiment to obtain observable droplet movement. Fig. 5a shows the initial droplet shape before the reductive potential was applied. Since the tilting angle (~7°) is much smaller than the critical angle (25°) required for movement of the droplet due to the buoyant force, the droplet remains pinned on the surface with only a slight deformation of the meniscus shapes on the uphill and downhill sides. Upon the application of a reductive potential to the PPy(DBS) electrode (Fig. 5b), the droplet started to deform further, particularly with the significant increase of the contact angle on the uphill side. It is due to the selective reduction of the PPy(DBS) layer under the unidirectional buoyant effect. As described in Section 3.1.1, when the reductive potential is applied, only the PPy(DBS) surface underneath the droplet would be fed by sodium ions from salt water, while the PPy(DBS) surface exposed to DCM remains oxidized (Fig. 5b′). Then, a surface tension gradient is set across the droplet boundary and the resultant Marangoni stress causes the contact angle on the uphill side to increase up to the advancing contact angle. On the downhill side, the increase of contact angle is not as dramatic as in the leveled configuration because of the unidirectional buoyant force in the tilted configuration. Such deformation reduces the contact diameter and the area, which results in the decrease of static friction on the droplet. Then, the buoyant force can overcome the static friction and lead the droplet to move uphill. However, after a slight uphill movement, the droplet stopped (Fig. 5c). This is because the droplet boundary on the uphill side now contacts with the initial oxidized PPy(DBS) surface, and no significant surface tension gradient (*i.e.*, Marangoni stress) is set across the droplet boundary at the new position (Fig. 5c′). Without the existence of the surface tension gradient, the contact angle reduces back to that of the oxidized state, which holds the droplet in its current position. On the downhill side, the droplet transitions to the homogeneously reduced PPy(DBS) surface with little surface tension gradient present, so that no significant deformation occurs either. Then, another deformation and movement occurred while the reductive potential continued to be applied (Fig. 5d and 5e). Since the reductive potential is continuously applied, the pre-oxidized PPy(DBS) area newly covered by the salt water droplet is reduced (Fig. 5d′). Then, it creates a surface tension gradient across the new droplet boundary and causes the droplet to deform and move uphill again (Fig. 5e′). This discrete behavior of the droplet deformation and movement continues until the droplet leaves the camera's visible area (Fig. 5f and 5f′).

**3.2.2** Water droplet manipulation by square pulse potentials. We also investigated the droplet manipulation by using a square pulse potential (−1.5 V to 0.6 V) in the tilted microchannel configuration to examine if the regulated oxidative potential (0.6 V) can serve as a stopping mechanism allowing programmable manipulation of the droplet movement. Fig. 6 shows the experimental results and schematics of the droplet behaviors. As shown in Fig. 5, a tilting angle of 7° was required to hold the droplet on the naturally oxidized PPy(DBS) surface. In contrast, when the oxidative potential (0.6

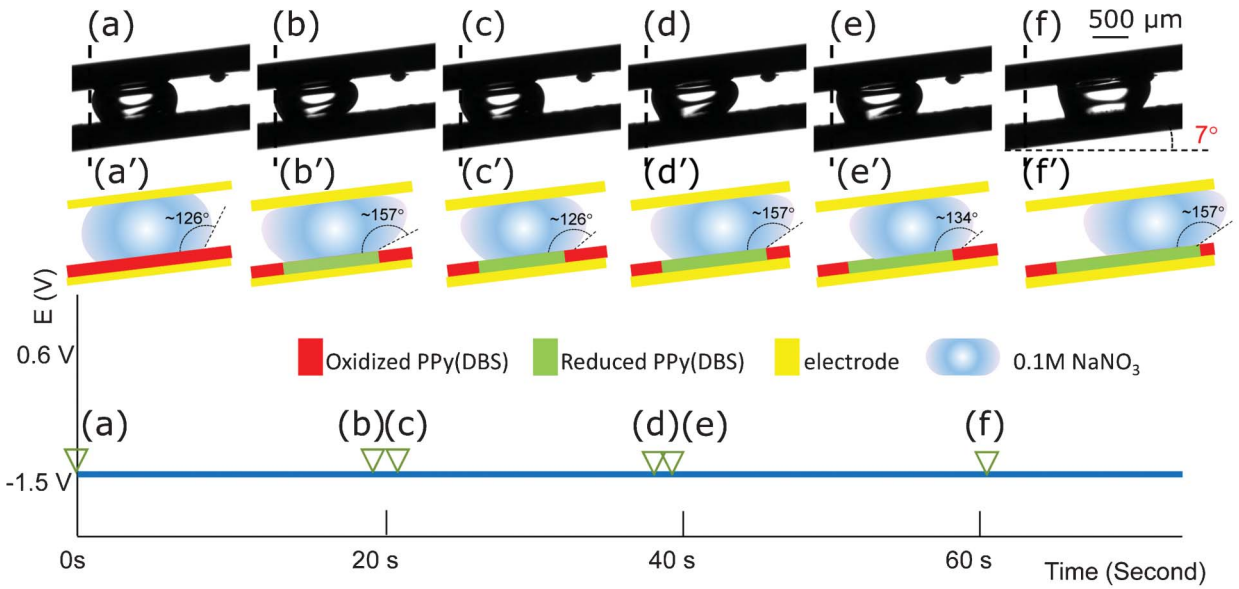


**Fig. 5** Top: captured images of a salt water droplet in a tilted microchannel within a DCM environment under a constant reductive potential (−1.5 V). Middle: Schematic of PPy(DBS) surface states and droplet deformation on the PPy(DBS) under a constant potential.

V) was applied to the PPy(DBS), the droplet was driven at the tilting angle of 4°, which was the minimum angle to obtain observable droplet movement. When the microchannel was initially tilted by 4°, a slight asymmetric deformation of a droplet occurred with the application of the oxidative potential (0.6 V) (Fig. 6a). The water droplet on the initially oxidative surface was pinned since the tilted angle (4°) was much less than the critical angle (25°) required for spontaneous movement by the buoyancy effect. Upon the application of the reductive potential (−1.5 V) to the PPy(DBS) layer, the water droplet was deformed and moved uphill (Fig. 6b–c). As demonstrated in Section 3.2.1, the application of a reductive

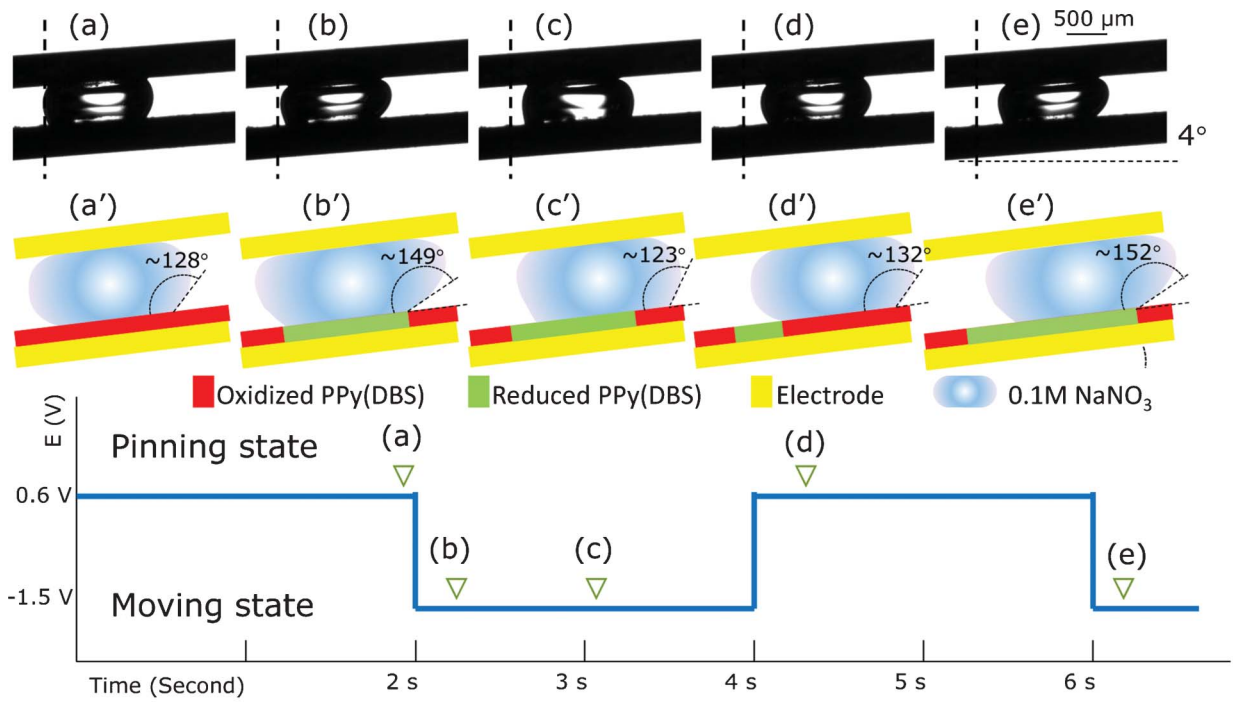


**Fig. 6** Top: schematics of droplet behavior. Center: captured images of a salt water droplet in a tilted (4°) microchannel immersed in a DCM environment under a square pulse potential (0.6 V to −1.5 V, pulse: 2 s). Bottom: elapsed timeframe *vs.* square pulse potential.

potential induces the droplet actuation due to the combined effects of Marangoni stress and buoyant force (Fig. 6b′–c′). When the potential was reverted and the initial oxidation voltage (0.6 V) was applied again, the droplet stopped moving and switched back to the initial pinning state (Fig. 6d). Compared to the case when a constant reductive potential was continuously applied where the droplet stopped for only a very short span (Fig. 5c and 5c′), the pinning state was clearly maintained for a programmable interval by keeping the oxidation voltage switched on (Fig. 6d′). It suggests that the oxidative potential can be utilized as an active stopping mechanism for the low-voltage droplet manipulation for digital microfluidics applications. When the reductive potential was applied again, the droplet was reactivated and resumed the movement (Fig. 6e and 6e′). In this way, by applying the regulated pulse potential, the droplet movement was precisely manipulated.

## 4. Conclusions

We have demonstrated that the ultra-low voltage (<1 V) redox process of the conjugated polymer PPy(DBS) can manipulate and actuate an aqueous droplet in a microchannel while immersed in an immiscible organic fluid. When a reductive potential was applied to the PPy(DBS) layer, the droplet contact angle significantly increased due to the Marangoni stress induced across the droplet contact boundary. When the reduction potential was prolonged, the sodium ions in the water droplet were radially diffused through the PPy(DBS) layer. The lateral ionic diffusion mitigated the Marangoni stress and caused the droplet to be pinned on the surface. In a level microchannel configuration where no asymmetric force was provided along the lateral direction, such combined effects resulted in the asymmetric deformation of the droplet into a funnel-like geometry along the vertical direction. However, along the lateral direction, it maintained symmetry and therefore no movement was observed. In the slightly tilted microchannel configuration, an asymmetric force was introduced to the droplet due to the buoyant force. When the Marangoni stress and the unidirectional buoyant force were combined *via* the redox process in the tilted configuration, the lateral transport of the droplet (volume: 2–3 μL, droplet diameter: ~1.5 μm) was attainable with the tilting angle as low as 4° (equivalent to the lateral buoyant force in the order of 10 μN). Movement of the water droplet was precisely controlled by applying a regulated square-pulse redox potential. The programmable electrochemical redox process using smart polymers will pave a new way for the ultra-low voltage digital microfluidics platform.

## Acknowledgements

This work has been supported in part by National Science Foundation awards (ECCS-1202269, DMR-0922522, EECS-1040007, ECCS-1104870, and EEC-1138244) and the Defence University Research Instrumentation Program (FA9550-11-1-0272). The authors also thank Dr. Wei Xu for his valuable comments in reviewing the paper.

## References

1 H. Stefan and Z. Roland, *Lab Chip*, 2007, **7**, 1094–1110.
2 G. M. Whitesides, *Nature*, 2006, **442**, 368–373.
3 H. A. Stone, A. D. Stroock and A. Ajdari, *Annu. Rev. Fluid Mech.*, 2004, **36**, 381–411.
4 T. M. Squires and S. R. Quake, *Rev. Mod. Phys.*, 2005, **77**, 977–1026.
5 S. Y. Teh, R. Lin, L. H. Hung and A. P. Lee, *Lab Chip*, 2008, **8**, 198.
6 M. Abdelgawad and A. R. Wheeler, *Adv. Mater.*, 2009, **21**, 920–925.
7 C. Quilliet and B. Berge, *Curr. Opin. Colloid Interface Sci.*, 2001, **6**, 34–39.
8 F. Mugele and J. C. Baret, *J. Phys.: Condens. Matter*, 2005, **17**, R705–R774.
9 J. S. Gaurav, T. O. Aaron, P. Y. C. Eric, C. W. Ming and J. K. Chang-Jin, *Lab Chip*, 2009, **9**, 1732–1739.
10 J. Berthier, P. Dubois, P. Clementz, P. Claustre, C. Peponnet and Y. Fouillet, *Sens. Actuators, A*, 2007, **134**, 471–479.
11 J. Lienemann, A. Greiner and J. G. Korvink, *IEEE Trans. Comput.-Aided Des. Integr. Circuits Syst.*, 2006, **25**, 234–247.
12 J. Isaksson, C. Tengstedt, M. Fahlman, N. Robinson and M. Berggren, *Adv. Mater.*, 2004, **16**, 316–320.
13 J. A. Halldorsson, S. J. Little, D. Diamond, G. Spinks and G. Wallace, *Langmuir*, 2009, **25**, 11137–11141.
14 M. Liu, F. Q. Nie, Z. Wei, Y. Song and L. Jiang, *Langmuir*, 2010, **26**, 3993–3997.
15 J. Isaksson, N. D. Robinson and M. Berggren, *Thin Solid Films*, 2006, **515**, 2003–2008.
16 G. G. Wallace, G. M. Spinks, L. A. P. Kane-Maguire and P. R. Teasdale, *Conductive Electroactive Polymers: Intelligent Polymer Systems*, CRC Press, Boca Raton, 2008.
17 E. Smela and N. Gadegaard, *J. Phys. Chem. B*, 2001, **105**, 9395–9405.
18 X. Wang and E. Smela, *J. Phys. Chem. C*, 2009, **113**, 359–368.
19 X. Wang and E. Smela, *J. Phys. Chem. C*, 2009, **113**, 369–381.
20 M. J. Higgins, P. J. Molino, Z. Yue and G. G. Wallace, *Chem. Mater.*, 2012, **24**, 828–839.
21 Y.-T. Tsai, C.-H. Choi, N. Gao and E.-H. Yang, *Langmuir*, 2011, **27**, 4249–4256.
22 J. Berthier, *Microdrops and Digital Microfluidics*, William Andrew Inc., Norwick, NY, 2008.
23 L. Malic, D. Brassard, T. Veres and M. Tabrizian, *Lab Chip*, 2010, **10**, 418–431.
24 J. Berthier and P. Silberzan, *Microfluidics for Biotechnology*, Artech House, Boston, 2006.
25 C. Y. Fan, Y. C. Tung, S. Takayama, E. Meyhöfer and K. Kurabayashi, *Adv. Mater.*, 2008, **20**, 1418–1423.
26 S.-K. Fan, H. Yang and W. Hsu, *Lab Chip*, 2010, **11**, 343–347.
27 I.F. Uchegbu and A. G. Schätzlein, *Polymers in Drug Delivery*, CRC Press, Boca Raton, FL, 2006.
28 R. B. Fair, *Microfluid. Nanofluid.*, 2007, **3**, 245.
29 E. Smela, *J. Micromech. Microeng.*, 1999, **9**, 1–18.

30 R. M. Torresi, S. I. Córdoba de Torresi, T. Matencio and M. A. De Paoli, *Synth. Met.*, 1995, **72**, 283–287.
31 T. Matencio, M. A. De Paoli, R. C. D. Peres, R. M. Torresi and S. I. Cordoba de Torresi, *Synth. Met.*, 1995, **72**, 59–64.
32 K. S. Teh, Y. Takahashi, Z. Yao and Y.-W. Lu, *Sens. Actuators, A*, 2009, **155**, 113–119.
33 Y. W. Lu, Y. Takahashi and K. S. Teh, Wettability switching technique of a biocompatible polymer for protein adhesion control, *Proceedings of the 22nd Annual IEEE International Conference on Micro Electro Mechanical Systems (IEEE-MEMS)*, Sorrento, Italy, January 25–29, 2009.
34 L. Xu, W. Chen, A. Mulchandani and Y. Yan, *Angew. Chem., Int. Ed.*, 2005, **44**, 6009–6012.
35 S. Skaarup, L. Bay, K. Vidanapathirana, S. Thybo, P. Tofte and K. West, *Solid State Ionics*, 2003, **159**, 143–147.
36 C. Priest, T. W. J. Albrecht, R. Sedev and J. Ralston, *Langmuir*, 2009, **25**, 5655–5660.
37 C.-T. Hsieh, F.-L. Wu and W.-Y. Chen, *J. Phys. Chem. C*, 2009, **113**, 13683–13688.



 